ROYAL SOCIETY
OF CHEMISTRY

PAPER

Check for updates

Highly efficient and stable binary all-polymer solar cells enabled by sequential deposition processing tuned microstructures†

Chaoyue Zhao,‡[a] Ruijie Ma, ‡*[b] Jiyeon Oh,[c] Lihong Wang,[a] Guoping Zhang,[a] Yajie Wang,[a] Siying He,[a] Liangxiang Zhu,[a] Changduk Yang,[c] Guangye Zhang*[a] and Gang Li *[b]

The power conversion efficiency (PCE) and operation stability of all-polymer solar cells (all-PSCs) are expected to be simultaneously pushed to a high level, that can be considered for further commercialization. Here the sequential processing (SqP) method is applied to process the PM6:PY-DT all-polymer system, while the control devices are made from the blend casting (BC) method. As a result, the efficiency rises to 16.5% in SqP devices from 15.8% of their BC counterparts, which is mainly caused by the improved fill factor (FF). Device physics study and morphology analysis reveal that optimized crystallinity and vertical phase separation result in suppressed charge recombination, higher charge collection and transport ability, which is responsible for PV performance improvement. In addition, operational stability is compared by maximal power point (MPP) tracking: the SqP device has a significantly longer time it takes to degrade to 80% of its initial PCE than the BC device, which could be attributed to the vertical composition distribution optimization realized by the two-step coating method. This work successfully demonstrates the effectiveness and promising future of using an SqP method to boost device performance for all-PSCs.

Introduction

Organic solar cells (OSCs) are one of the most promising green energy technologies, to realize carbon neutrality.[1–6] In the past few decades, researchers put tremendous effort into pursuing high power conversion efficiency (PCE) for OSCs, and as a consequence values >19% have been reported by many different groups.[7–17] However, the fruitful development solely of efficiency enhancement cannot fulfill the requirement of commercialized photovoltaic (PV) cargo, where the device stability matters equally importantly.[18–20] Due to the intrinsic disadvantages of small molecules in morphology stability, OSC devices with superior

stability are more feasible when they contain an active layer with both polymeric donor(s) and acceptor(s). In other words, all-polymer solar cells (all-PSCs) have potential in the OSC field.

To date, the main challenge of all-PSCs is their relative low efficiencies compared to their small molecular counterparts. Though this gap has been successfully alleviated by the new concept of a polymerized small molecular acceptor (PSMA), specifically PCEs are now over 16% in multiple cases.[21–29] Nonetheless, the operational and mechanical stability difficulties come back again, due to PSMAs partially inheriting the properties of small molecules.[30–33] Since current PSMA-type materials are the most promising candidates for high-efficiency, more efforts in boosting device stability are required that rely not only on chemistry innovation, but also effective device fabrication methods.

Compared with traditional blend casting (BC), recently more and more exciting PCE values have been achieved using a sequential processing (SqP) method,[34–36] initially explored in the PCBM era. Not only is simple efficiency enhancement reported using the SqP method, other advantages like high transparency and improved mechanical durability were also found.[37–40] All these achievements suggest tuning the nanostructure of the active layer using an SqP method in both horizontal and vertical directions at the same time is a promising choice to realize high PCE and stability for all-PSCs.

Herein, we applied the SqP method to an all-polymer photo-voltaic blend (PM6 as donor, PY-DT as acceptor) – which has

[a] *College of New Materials and New Energies, Shenzhen Technology University, Shenzhen 518118, China. E-mail: zhangguangye@sztu.edu.cn*

[b] *Department of Electronic and Information Engineering, Research Institute for Smart Energy (RISE), Guangdong-Hong Kong-Macao (GHM) Joint Laboratory for Photonic-Thermal-Electrical Energy Materials and Devices, The Hong Kong Polytechnic University, Hung Hom, Kowloon, Hong Kong, 999077, China. E-mail: ruijie.ma@polyu.edu.hk, gang.w.li@polyu.edu.hk*

[c] *Department of Energy Engineering, School of Energy and Chemical Engineering, Perovtronics Research Center, Low Dimensional Carbon Materials Center, Ulsan National Institute of Science and Technology (UNIST), 50 UNIST-gil, Ulju-gun, Ulsan, 44919, South Korea*

† Electronic supplementary information (ESI) available. See DOI: https://doi.org/10.1039/d2tc04142a

‡ Equal contribution.

This journal is © The Royal Society of Chemistry 2022

J. Mater. Chem. C, 2022, **10**, 17899–17906 | **17899**

already been reported with high PCEs in BC processed devices[41] – to seek a chance of achieving simultaneously efficient and stable all-PSCs. As a result, the SqP enabled PM6:PY-DT based device delivers an optimal PCE of 16.5% while that of the BC processed device is 15.8%. The efficiency improvement comes from concurrently increased open-circuit voltage (V_{OC}), short-circuit current density (J_{SC}) and fill factor (FF). Among them, the betterment of FF is the main contributor. Device physics study supports that the SqP PM6:PY-DT blend film exhibits significantly enhanced charge mobility, especially the electron mobility, and correspondingly improved charge collection and suppressed recombination. Morphology characterization clearly shows the graded morphology achieved by SqP, as well as more ordered crystallization, which is consistent with mobility enhancement and recombination suppression. As a final stage, device stabilities of two types of solar cells are evaluated by placing them under maximal power point (MPP) tracking under a white LED with 1 sun intensity. Compared with the BC device, the SqP one exhibits well maintained V_{OC} and FF, thereby obviously longer T80 (the time it takes for a device to degrade to 80% of its initial PCE). It is believed that optimized vertical phase segregation contributes to the stability enhancement, according to film-depth-dependent light absorption spectra (FLAS). This paper presents decent PCE with distinguishable improvement for target devices together with better operation stability, proving the effectiveness and prospect of the SqP method in boosting PV performance for all-PSCs.

Results and discussion

The chemical structures of donor and acceptor materials PM6 and PY-DT are shown in Fig. 1(a), together with the energy level distribution: highest occupied molecular orbit (HOMO) and lowest unoccupied molecular orbit (LUMO), of all materials applied in this research in Fig. 1(b).[41] All of them are obtained

from commercial paths and used without further purification. The fabrication schematic diagram of BC and SqP devices are illustrated in Fig. 1(c), with a conventional structure of ITO/PEDOT:PSS/active layer/PNDIT-F3N/Ag.

The normalized ultraviolet-visible (UV-vis) absorption spectra of neat films of PM6 and PY-DT and their blended films fabricated using BC or SqP methods, are plotted in Fig. 2(a) and (b), respectively. Highly close intensities of 0–0 and 0–1 vibrational peaks indicate that PM6 in a film state exhibits H- and J-aggregation simultaneously. PY-DT's absorption peak locates at *ca.* 800 nm, which is generally complementary to that of PM6. The BC and SqP blend films are generally the same but with some minor differences, which implies SqP might bring some delicate adjustment in film morphology.

The device performance comparison is shown in Fig. 2(c), with the current density *versus* voltage (*J–V*) characteristics, and in Table 1. The fabrication details can be found in the ESI.† Accordingly, BC devices display a PCE of 15.8%, with a V_{OC} of 0.960 V, a J_{SC} of 23.2 mA cm^{-2} and an FF of 70.8%. Though the absolute value here is lower than what was reported in the reference, it could be reasonable once we consider the polymer batch differences and processing solvent variation.[41] Herein, we chose toluene, an eco-friendly solvent, instead of chloroform which was used before. The SqP devices demonstrate optimal efficiency as high as 16.5%, among the highest level of PCEs for non-halogenated solvent processed all-PSCs.[42–48] The increase of PCE mainly comes from FF improvement, but also partially benefits from slightly higher V_{OC} and J_{SC}. In addition, the external quantum efficiency (EQE) spectra of these two types of devices are measured and depicted in Fig. 2(d). The corresponding integral current density values are 22.5 and 22.7 mA cm^{-2}, respectively (also listed in Table 1). Therein, the measurement error should be smaller than 4% in this report.

To figure out the underlying reason for FF enhancement of SqP devices, the charge mobility variation is firstly investigated

Fig. 1 (a) Chemical structures of polymer donor PM6 and polymer acceptor PY-DT. (b) Energy level distribution of materials in our devices. (c) Processing schematic diagram of BC and SqP methods.

17900 | *J. Mater. Chem. C*, 2022, **10**, 17899–17906

This journal is © The Royal Society of Chemistry 2022

Fig. 2 UV-vis spectra of (a) PM6 and PY-DT neat films, and (b) BC and SqP blend films. (c) $J–V$ characteristics and (d) EQE spectra.

Table 1 Summary of photovoltaic parameters for PM6 and PY-DT based all-PCSs processed from different methods, measured under AM 1.5 G illumination at 100 mW cm^{-2}

Active layer	V_{OC} [V]	J_{SC} [mA cm^{-2}]	J_{EQE} [mA cm^{-2}]	FF	PCE^a [%]	μ_h [cm^2 V^{-1} s^{-1}]	μ_e [cm^2 V^{-1} s^{-1}]
BC	0.962 ± 0.001 (0.960)	23.1 ± 0.3 (23.2)	22.5	0.703 ± 0.005 (0.708)	15.6 ± 0.2 (15.8)	5.83 × 10^{-4}	5.01 × 10^{-4}
SqP	0.964 ± 0.002 (0.964)	23.2 ± 0.2 (23.6)	22.7	0.728 ± 0.004 (0.725)	16.32 ± 0.10 (16.5)	7.30 × 10^{-4}	7.84 × 10^{-4}

^{a} The standard deviations are based on measurements of over at least ten independent devices.

by the space charge limited current (SCLC) method. The calculation and experimental details are also given in ESI.† The hole-only and electron-only device results are presented in Fig. 3(a) and (b), and are noted with fitted values for hole mobility and electron mobility (μ_h and μ_e). The μ_h increases from 5.83 × 10^{-4} cm^2 V^{-1} s^{-1} to 7.30 × 10^{-4} cm^2 V^{-1} s^{-1} for hole-only devices; and 7.84 × 10^{-4} cm^2 V^{-1} s^{-1} from 5.01 × 10^{-4} cm^2 V^{-1} s^{-1} for electron-only devices. Accordingly, the SqP device promotes the electron transport ability of the active layer significantly, and in a smaller way for hole transport. Then the general charge transport of the SqP film is obviously improved, which is supposed to be beneficial for achieving higher FF (suppressed charge recombination and more efficient charge extraction).

Next, the recombination dynamics is quantitatively studied by transient photovoltage (TPV) measurement. The mono-exponential

decay of the TPV signal is shown in Fig. 3(c), where the fitted recombination lifetime for the BC device is 2.00 μs and that of the SqP device is 2.64 μs. The prolonged value here allows the reduction of recombination and the boosting of the FF. Meanwhile, the charge extraction characteristics are compared by transient photocurrent (TPC). Fig. 3(d) shows that the extraction lifetime of the SqP device is a little shorter than its BC counterpart (0.15 μs vs. 0.17 μs). Thereby, the vertically optimized film possibly facilitates the charge collection, which might contribute to FF. Apart from the direct evidence provided by the TPV and TPC experiments, the light intensity dependent J_{SC}/V_{OC} and dark current devices are also measured to obtain more side supports in Fig. S1 (from a to c) (ESI†). The bimolecular recombination rates are nearly identical, while the diode ideality factor for an SqP device under light and dark, is closer to 1 compared with that of the BC devices. These
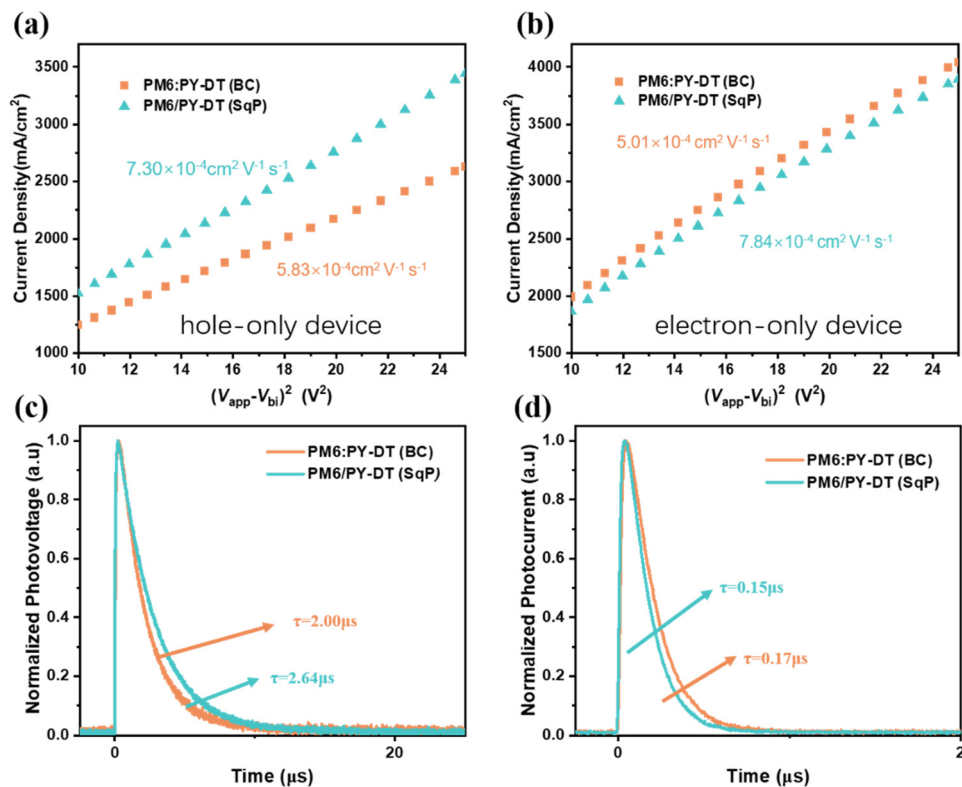
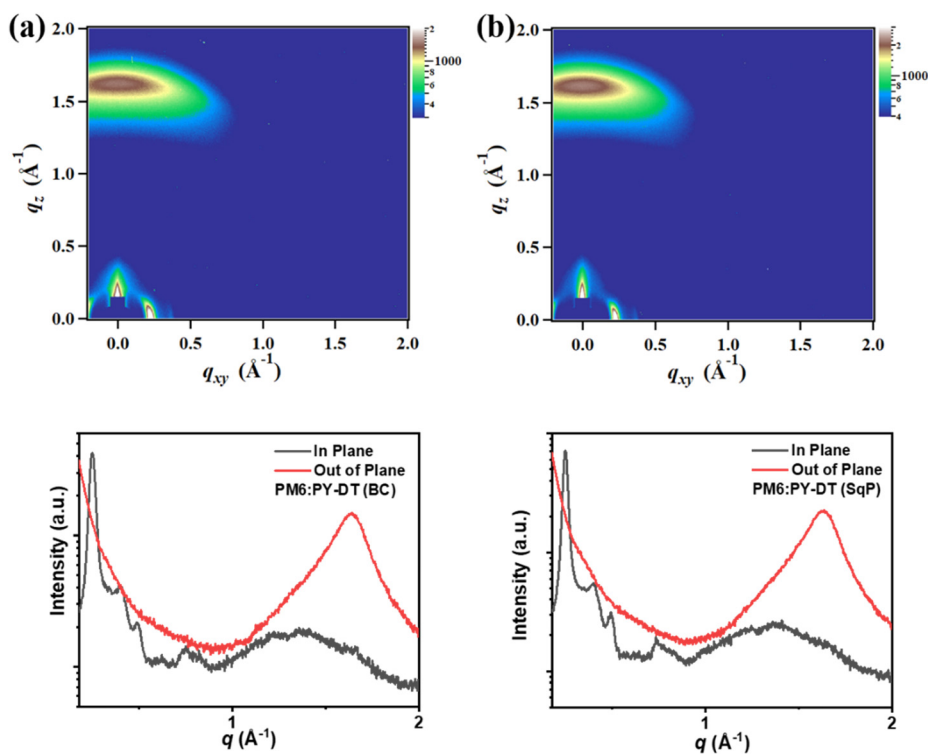**Fig. 3** (a) Hole-only and (b) electron-only device results; (c) TPV + (d) TPC curves.

Fig. 4 2D-GIWAXS patterns and line-cuts of (a) BC and (b) SqP blend films.

17902 | *J. Mater. Chem. C*, 2022, **10**, 17899–17906

This journal is © The Royal Society of Chemistry 2022

results suggest that the SqP device operates more like an ideal diode than a BC device does, which is intrinsically better for pursuing high FF.

Then the morphology study is carried out by atomic force microscopy (AFM) as the first stage. The corresponding height images of PM6, PY-DT neat films, and blend films processed from BC and SqP methods are displayed in Fig. S2a–d (ESI†), it is shown that PM6 has a smoother surface than PY-DT, but the SqP surface is smoother than the BC one, indicating more PM6 aggregates on the top part of the *ca.* 100 nm thick film. This is contradictory to our hypothesis that PY-DT should take the dominant position at the top. However, such phenomenon is also observed in a recent report,[49] and can be rationalized once we consider the composition migration driven by thermal annealing or a solvent additive's slow evaporation.[50–53] The AFM experiments only give us a vague and preliminary impression of film morphology. For further understanding of molecular packing and crystallinity change in active layers, grazing incidence wide-angle X-ray scattering (GIWAXS) technology is applied.[54–57] The 2D patterns and derived line cuts of BC and SqP films are shown in Fig. 4, with calculated parameters of (010) diffraction peaks presented in Table S1 (ESI†). The molecular packing mode is basically the same for two types of active layers, but the SqP can promote the crystallization quality of π–π stacking: the coherence length increases from 29.6 to 31.4 Å. More ordered π–π packing with similar diffraction intensity implies that the charge transport property could be improved.

Besides, the vertical distribution of PM6 and PY-DT is quantitatively studied by the film-depth-dependent light absorption (FLAS) characterization.[58] The raw results are

illustrated in Fig. 5(a) and (b) and Fig. S3a, b (ESI†), respectively, for BC and SqP active layers. Meanwhile, the corresponding composition weight ratio of PM6 and PY-DT at different depths in the films are plotted in Fig. 5(c) and (d). It is observed in the BC film, that PY-DT assembles at the top surface and then immediately shows a content drop with increasing depth. Further monotonous enhancement of the PY-DT ratio follows the weight ratio of 1:1.2 for donor and acceptor. In contrast, the SqP film contains PY-DT's vertical distribution with continuous high ratio in the top part of the film, which is beneficial to forming more phases that are continuous vertically, facilitating the charge transport and collection. Based on this analysis, the advantage of SqP is further demonstrated. In addition to these results, one more important issue is to rationally claim why such vertical distribution appears: (i) the polymerized Y-series acceptor usually has a higher surface free energy than PM6, which supports its agglomeration at the bottom top of the active layer in both BC and SqP films; (ii) the polymer acceptor (PY-DT herein) has better solubility in solvent additive 1-chloronaphthalene (1-CN), which means it will be partially deposited after the removal of the main solvent toluene, and shows a sudden content ratio increase at the top surface in BC films.[59–61]

Finally, the operational stability of the BC and SqP devices are evaluated by placing them under maximal power point (MPP) tracking (Fig. 6). After 100 hours, the BC device degrades to 80% of its initial PCE, and it keeps dropping to *ca.* 70% the initial PCE after 160 hours under illumination. The SqP device, on the contrary, keeps the PCE level at about 95% the initial PCE after 160 hours degradation. Clearly the SqP method is helpful to achieve highly stable all-PSCs, implying the very

Fig. 5 FLAS of (a) BC and (b) SqP blended films. Calculated vertical ratio of PM6 and PY-DT for (c) BC and (d) SqP blended films.
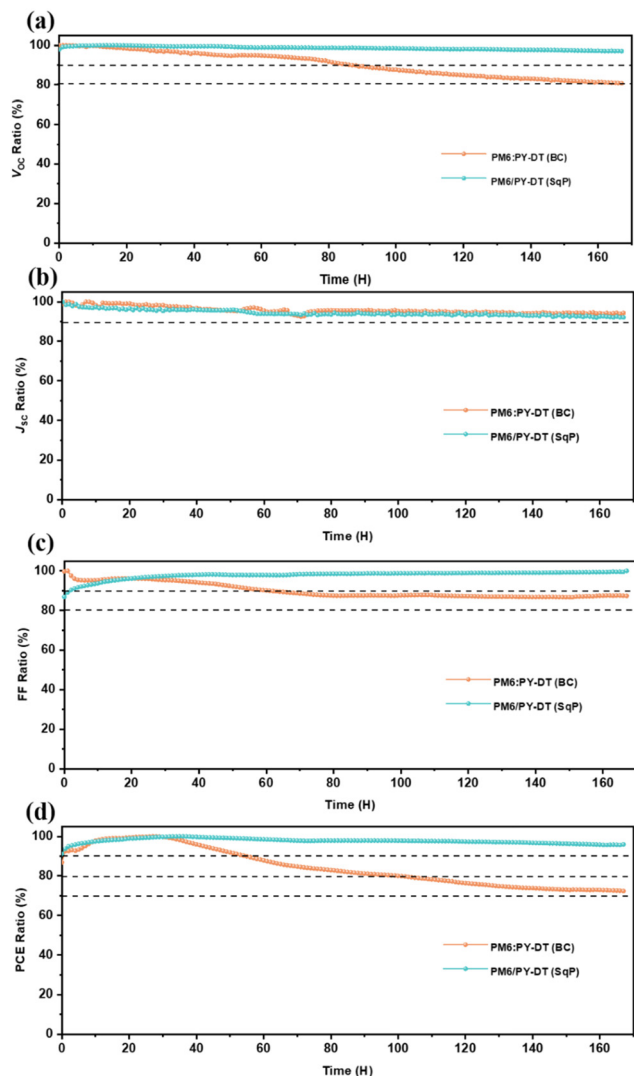
Fig. 6 MPP tracking results for BC and SqP devices: (a) V_{OC}, (b) J_{SC}, (c) FF and (d) PCE.

to compare the performance, and seek a chance of achieving better efficiency and stability simultaneously. As a result, the BC device demonstrates a PCE of 15.8% (lower than reported values, possibly due to batch differences and non-halogen solvents as the processing medium), and the SqP has higher efficiency of 16.5% which is mainly contributed by the enhancement of FF. Further characterization reveals that optimized vertical distribution and crystallinity of the active layer leads to promoted charge transport and suppressed recombination as well as charge collection, which well supports the PV performance improvement. Meanwhile, the stability is considered using MPP tracking results, which show that the SqP device is obviously more stabe than its BC counterpart, which can be understood by the tuned vertical composition distribution. This paper further emphasizes the prospect and effectiveness of the SqP method in pursuing better device performance for all-PSCs.

Author contributions

Conflicts of interest

There are no conflicts to declare.

Acknowledgements

promising future of using this fabrication to propel the commercialization of OSCs.

Principally, it is also understandable for improved PCE in SqP devices – from the point of thermodynamics[62,63] – that morphology degradation of the donor–acceptor heterojunction involves complete separation from each other since they have very different surface free energies. Besides, the larger surface free energy acceptor will concentrate at the bottom, and PM6 should agglomerate at the top. The SqP film successfully tunes the vertical distribution of PM6 and PY-DT, which increases the difficulty to achieve the final balance of thermodynamics, therefore better device stability.

Conclusion

In summary, we choose a reported highly efficient binary all-polymer photovoltaic blend PM6:PY-DT as the research object, and fabricate a series of devices based on BC and SqP methods,

17904 | *J. Mater. Chem. C*, 2022, **10**, 17899–17906

This journal is © The Royal Society of Chemistry 2022

References

1 A. J. Heeger, *Adv. Mater.*, 2014, **26**, 10–28.
2 Y. He, N. Li, T. Heumüller, J. Wortmann, B. Hanisch, A. Aubele, S. Lucas, G. Feng, X. Jiang, W. Li, P. Bäuerle and C. J. Brabec, *Joule*, 2022, **6**, 1160–1171.
3 Q. Bai, Q. Liang, H. Li, H. Sun, X. Guo and L. Niu, *Aggregate*, 2022, e281.
4 C. Cui and Y. Li, *Aggregate*, 2021, **2**, e31.
5 M. Gao, W. Wang, J. Hou and L. Ye, *Aggregate*, 2021, **2**, e46.
6 Z. Luo, R. Ma, J. Yu, H. Liu, T. Liu, F. Ni, J. Hu, Y. Zou, A. Zeng, C.-J. Su, U-S. Jeng, X. Lu, F. Gao, C. Yang and H. Yan, *Natl. Sci. Rev.*, 2022, **9**(7), DOI: **10.1093/nsr/nwac076**.
7 L. Zhu, M. Zhang, J. Xu, C. Li, J. Yan, G. Zhou, W. Zhong, T. Hao, J. Song, X. Xue, Z. Zhou, R. Zeng, H. Zhu, C.-C. Chen, R. C. I. MacKenzie, Y. Zou, J. Nelson, Y. Zhang, Y. Sun and F. Liu, *Nat. Mater.*, 2022, **21**, 656–663.
8 Y. Cui, Y. Xu, H. Yao, P. Bi, L. Hong, J. Zhang, Y. Zu, T. Zhang, J. Qin, J. Ren, Z. Chen, C. He, X. Hao, Z. Wei and J. Hou, *Adv. Mater.*, 2021, **33**, 2102420.
9 R. Ma, C. Yan, J. Yu, T. Liu, H. Liu, Y. Li, J. Chen, Z. Luo, B. Tang, X. Lu, G. Li and H. Yan, *ACS Energy Lett.*, 2022, **7**, 2547–2556.
10 W. Gao, F. Qi, Z. Peng, F. R. Lin, K. Jiang, C. Zhong, W. Kaminsky, Z. Guan, C.-S. Lee, T. J. Marks, H. Ade and A. K. Y. Jen, *Adv. Mater.*, 2022, **34**, 2202089.
11 Y. Wei, Z. Chen, G. Lu, N. Yu, C. Li, J. Gao, X. Gu, X. Hao, G. Lu, Z. Tang, J. Zhang, Z. Wei, X. Zhang and H. Huang, *Adv. Mater.*, 2022, **34**, 2204718.
12 L. Zhan, S. Yin, Y. Li, S. Li, T. Chen, R. Sun, J. Min, G. Zhou, H. Zhu, Y. Chen, J. Fang, C.-Q. Ma, X. Xia, X. Lu, H. Qiu, W. Fu and H. Chen, *Adv. Mater.*, 2022, 2206269.
13 R. Sun, Y. Wu, X. Yang, Y. Gao, Z. Chen, K. Li, J. Qiao, T. Wang, J. Guo, C. Liu, X. Hao, H. Zhu and J. Min, *Adv. Mater.*, 2022, **34**, 2110147.
14 J. Wang, M. Zhang, J. Lin, Z. Zheng, L. Zhu, P. Bi, H. Liang, X. Guo, J. Wu, Y. Wang, L. Yu, J. Li, J. Lv, X. Liu, F. Liu, J. Hou and Y. Li, *Energy Environ. Sci.*, 2022, **15**, 1585–1593.
15 Z. Zheng, J. Wang, P. Bi, J. Ren, Y. Wang, Y. Yang, X. Liu, S. Zhang and J. Hou, *Joule*, 2022, **6**, 171–184.
16 R. Ma, C. Yan, P. W.-K. Fong, J. Yu, H. Liu, J. Yin, J. Huang, X. Lu, H. Yan and G. Li, *Energy Environ. Sci.*, 2022, **15**, 2479–2488.
17 L. Zhan, S. Li, Y. Li, R. Sun, J. Min, Y. Chen, J. Fang, C.-Q. Ma, G. Zhou, H. Zhu, L. Zuo, H. Qiu, S. Yin and H. Chen, *Adv. Energy Mater.*, 2022, 2201076.
18 P. Cheng and X. W. Zhan, *Chem. Soc. Rev.*, 2016, **45**, 2544–2582.
19 L. Duan and A. Uddin, *Adv. Sci.*, 2020, **7**, 1903259.
20 M. Gao, Y. Liu, K. Xian, Z. Peng, K. Zhou, J. Liu, S. Li, F. Xie, W. Zhao, J. Zhang, X. Jiao and L. Ye, *Aggregate*, 2022, e190.
21 D. Zhou, C. Liao, S. Peng, X. Xu, Y. Guo, J. Xia, H. Meng, L. Yu, R. Li and Q. Peng, *Adv. Sci.*, 2022, **9**, 2202022.
22 G. Sun, X. Jiang, X. Li, L. Meng, J. Zhang, S. Qin, X. Kong, J. Li, J. Xin, W. Ma and Y. Li, *Nat. Commun.*, 2022, **13**, 5267.

23 R. Ma, K. Zhou, Y. Sun, T. Liu, Y. Kan, Y. Xiao, T. A. Dela Peña, Y. Li, X. Zou, Z. Xing, Z. Luo, K. S. Wong, X. Lu, L. Ye, H. Yan and K. Gao, *Matter*, 2022, **5**, 725–734.
24 C. Zhao, L. Wang, G. Zhang, Y. Wang, R. Hu, H. Huang, M. Qiu, S. Li and G. Zhang, *Molecules*, 2022, **27**, 5739.
25 J. Song, Y. Li, Y. Cai, R. Zhang, S. Wang, J. Xin, L. Han, D. Wei, W. Ma, F. Gao and Y. Sun, *Matter*, 2022, **5**, 4047.
26 T. Liu, T. Yang, R. Ma, L. Zhan, Z. Luo, G. Zhang, Y. Li, K. Gao, Y. Xiao, J. Yu, X. Zou, H. Sun, M. Zhang, T. A. Dela Peña, Z. Xing, H. Liu, X. Li, G. Li, J. Huang, C. Duan, K. S. Wong, X. Lu, X. Guo, F. Gao, H. Chen, F. Huang, Y. Li, Y. Li, Y. Cao, B. Tang and H. Yan, *Joule*, 2021, **5**, 914–930.
27 Q. Fan, R. Ma, W. Su, Q. Zhu, Z. Luo, K. Chen, Y. Tang, F. R. Lin, Y. Li, H. Yan, C. Yang, A. K. Y. Jen and W. Ma, *Carbon Energy*, 2022, DOI: **10.1002/cey2.267**.
28 J. Wang, Y. Cui, Y. Xu, K. Xian, P. Bi, Z. Chen, K. Zhou, L. Ma, T. Zhang, Y. Yang, Y. Zu, H. Yao, X. Hao, L. Ye and J. Hou, *Adv. Mater.*, 2022, **34**, 2205009.
29 H. Sun, B. Liu, Y. Ma, J.-W. Lee, J. Yang, J. Wang, Y. Li, B. Li, K. Feng, Y. Shi, B. Zhang, D. Han, H. Meng, L. Niu, B. J. Kim, Q. Zheng and X. Guo, *Adv. Mater.*, 2021, **33**, 2102635.
30 K. Zhou, K. Xian, Q. Qi, M. Gao, Z. Peng, J. Liu, Y. Liu, S. Li, Y. Zhang, Y. Geng and L. Ye, *Adv. Funct. Mater.*, 2022, **32**, 2201781.
31 Q. Fan, R. Ma, T. Liu, J. Yu, Y. Xiao, W. Su, G. Cai, Y. Li, W. Peng, T. Guo, Z. Luo, H. Sun, L. Hou, W. Zhu, X. Lu, F. Gao, E. Moons, D. Yu, H. Yan and E. Wang, *Sci. China: Chem.*, 2021, **64**, 1380–1388.
32 S. Yao, T. Yang, X. Shen, T. Li, B. Huang, H. Liu, X. Lu, T. Liu and B. Zou, *J. Mater. Chem. C*, 2022, **10**, 9723–9729.
33 Y. Wu, Q. Fan, B. Fan, F. Qi, Z. Wu, F. R. Lin, Y. Li, C.-S. Lee, H. Y. Woo, H.-L. Yip and A. K. Y. Jen, *ACS Energy Lett.*, 2022, **7**, 2196–2202.
34 Q. Wu, W. Wang, Y. Wu, Z. Chen, J. Guo, R. Sun, J. Guo, Y. Yang and J. Min, *Adv. Funct. Mater.*, 2021, **31**, 2010411.
35 Y. Zhang, K. Liu, J. Huang, X. Xia, J. Cao, G. Zhao, P. W. K. Fong, Y. Zhu, F. Yan, Y. Yang, X. Lu and G. Li, *Nat. Commun.*, 2021, **12**, 4815.
36 D.-H. Lee, Y. M. Yang, J. You, E. Richard and G. Li, *Nanotechnology*, 2014, **25**, 295401.
37 Y. Song, K. Zhang, S. Dong, R. Xia, F. Huang and Y. Cao, *ACS Appl. Mater. Interfaces*, 2020, **12**, 18473–18481.
38 Y. Cai, Q. Li, G. Lu, H. S. Ryu, Y. Li, H. Jin, Z. Chen, Z. Tang, G. Lu, X. Hao, H. Y. Woo, C. Zhang and Y. Sun, *Nat. Commun.*, 2022, **13**, 2369.
39 B. Li, X. Zhang, Z. Wu, J. Yang, B. Liu, Q. Liao, J. Wang, K. Feng, R. Chen, H. Y. Woo, F. Ye, L. Niu, X. Guo and H. Sun, *Sci. China: Chem.*, 2022, **65**, 1157–1163.
40 Q. Zhu, J. Xue, G. Lu, B. Lin, H. B. Naveed, Z. Bi, G. Lu and W. Ma, *Nano Energy*, 2022, **97**, 107194.
41 Y. Li, J. Song, Y. Dong, H. Jin, J. Xin, S. Wang, Y. Cai, L. Jiang, W. Ma, Z. Tang and Y. Sun, *Adv. Mater.*, 2022, **34**, 2110155.
42 T. Yang, S. Yao, T. Liu, B. Huang, Y. Xiao, H. Liu, X. Lu and B. Zou, *ACS Appl. Mater. Interfaces*, 2022, **14**, 29956–29963.

This journal is © The Royal Society of Chemistry 2022

J. Mater. Chem. C, 2022, **10**, 17899–17906 | **17905**

43 C. Zhu, Z. Li, W. Zhong, F. Peng, Z. Zeng, L. Ying, F. Huang and Y. Cao, *Chem. Commun.*, 2021, **57**, 935–938.

44 K. Hu, C. Zhu, K. Ding, S. Qin, W. Lai, J. Du, J. Zhang, Z. Wei, X. Li, Z. Zhang, L. Meng, H. Ade and Y. Li, *Energy Environ. Sci.*, 2022, **15**, 4157.

45 J. Zhang, T. Jia, C.-H. Tan, K. Zhang, M. Ren, S. Dong, Q. Xu, F. Huang and Y. Cao, *Sol. RRL*, 2021, **5**, 2100076.

46 B. Liu, H. Sun, J.-W. Lee, J. Yang, J. Wang, Y. Li, B. Li, M. Xu, Q. Liao, W. Zhang, D. Han, L. Niu, H. Meng, B. J. Kim and X. Guo, *Energy Environ. Sci.*, 2021, **14**, 4499–4507.

47 T. Jia, J. Zhang, H. Tang, J. Jia, K. Zhang, W. Deng, S. Dong and F. Huang, *Chem. Eng. J.*, 2022, **433**, 133575.

48 J. Song, Y. Li, Y. Cai, R. Zhang, S. Wang, J. Xin, L. Han, D. Wei, W. Ma, F. Gao and Y. Sun, *Matter*, 2022, **5**, 4047.

49 C. He, Y. Pan, G. Lu, B. Wu, X. Xia, C.-Q. Ma, Z. Chen, H. Zhu, X. Lu, W. Ma, L. Zuo and H. Chen, *Adv. Mater.*, 2022, **34**, 2203379.

50 C. McDowell, M. Abdelsamie, M. F. Toney and G. C. Bazan, *Adv. Mater.*, 2018, **30**, 1707114.

51 R. Ma, J. Yu, T. Liu, G. Zhang, Y. Xiao, Z. Luo, G. Chai, Y. Chen, Q. Fan, W. Su, G. Li, E. Wang, X. Lu, F. Gao, B. Tang and H. Yan, *Aggregate*, 2022, **3**, e58.

52 S. Bao, H. Yang, H. Fan, J. Zhang, Z. Wei, C. Cui and Y. Li, *Adv. Mater.*, 2021, **33**, 2105301.

53 H. Chen, R. Zhang, X. Chen, G. Zeng, L. Kobera, S. Abbrent, B. Zhang, W. Chen, G. Xu, J. Oh, S.-H. Kang, S. Chen, C. Yang, J. Brus, J. Hou, F. Gao, Y. Li and Y. Li, *Nat. Energy*, 2021, **6**, 1045–1053.

54 X. Jiang, P. Chotard, K. Luo, F. Eckmann, S. Tu, M. A. Reus, S. Yin, J. Reitenbach, C. L. Weindl, M. Schwartzkopf, S. V. Roth and P. Müller-Buschbaum, *Adv. Energy Mater.*, 2022, **12**, 2103977.

55 J. Rivnay, S. C. B. Mannsfeld, C. E. Miller, A. Salleo and M. F. Toney, *Chem. Rev.*, 2012, **112**, 5488–5519.

56 Z. Luo, Y. Gao, H. Lai, Y. Li, Z. Wu, Z. Chen, R. Sun, J. Ren, C. E. Zhang, F. He, H. Woo, J. Min and C. Yang, *Energy Environ. Sci.*, 2022, **15**, 4601.

57 R. Ma, T. Yang, Y. Xiao, T. Liu, G. Zhang, Z. Luo, G. Li, X. Lu, H. Yan and B. Tang, *Energy Environ. Mater.*, 2022, **5**, 977–985.

58 T. Xiao, J. Wang, S. Yang, Y. Zhu, D. Li, Z. Wang, S. Feng, L. Bu, X. Zhan and G. Lu, *J. Mater. Chem. A*, 2020, **8**, 401–411.

59 Y. Zhang, B. Wu, Y. He, W. Deng, J. Li, J. Li, N. Qiao, Y. Xing, X. Yuan, N. Li, C. J. Brabec, H. Wu, G. Lu, C. Duan, F. Huang and Y. Cao, *Nano Energy*, 2022, **93**, 106858.

60 Z. Li, Y. Liang, X. Qian, L. Ying and Y. Cao, *Chem. Eng. J.*, 2022, **446**, 136877.

61 Z. Luo, T. Liu, R. Ma, Y. Xiao, L. Zhan, G. Zhang, H. Sun, F. Ni, G. Chai, J. Wang, C. Zhong, Y. Zou, X. Guo, X. Lu, H. Chen, H. Yan and C. Yang, *Adv. Mater.*, 2020, **32**, 2005942.

62 Z. Wang, K. Gao, Y. Kan, M. Zhang, C. Qiu, L. Zhu, Z. Zhao, X. Peng, W. Feng, Z. Qian, X. Gu, A. K. Y. Jen, B. Z. Tang, Y. Cao, Y. Zhang and F. Liu, *Nat. Commun.*, 2021, **12**, 332.

63 R. Ma, T. Liu, Z. Luo, K. Gao, K. Chen, G. Zhang, W. Gao, Y. Xiao, T.-K. Lau, Q. Fan, Y. Chen, L.-K. Ma, H. Sun, G. Cai, T. Yang, X. Lu, E. Wang, C. Yang, A. K. Y. Jen and H. Yan, *ACS Energy Lett.*, 2020, **5**, 2711–2720.